

Particle production azimuthal asymmetries in a clustering of color sources model

I. Bautista[‡], L. Cunqueiro ^{*‡}, J. Dias de Deus ^{†‡} and C. Pajares [‡]

December 3, 2018

Abstract

The collective interactions of many partons in the first stage of the collisions is the usual accepted explanation of the sizable elliptical flow. The clustering of color sources provides a framework of partonic interactions. In this scheme, we show a reasonable agreement with RHIC data for $p_T < 1.5$ GeV/c in both the dependence of v_2 on transverse momentum and in the shape of the nuclear modified factor on the azimuthal angle for different centralities. We show the predictions at LHC energies for Pb-Pb. In the case of proton-proton collisions a sizable v_2 is obtained at this energy.

1 Introduction

A major breakthrough was the discovery by RHIC experiments of a large elliptic flow v_2 [1][2][3][4] [5][6][7][8][9]. A non vanishing anisotropic flow exist only if the particles measured in the final state depend not only on the physical conditions realized locally at their production point, but if particle production does also depend on the global event geometry. In a relativistic local theory, this non local information can only emerge as a collective effect, requiring interactions between the relevant degrees of freedom, localized at

*Laboratori Nazionali di Frascati, Via E.Fermi 40, 00044 Roma

†CENTRA, Departamento de Física, IST, Av. Rovisco Pais, 1049-001 Lisboa, Portugal

‡IGFAE and Departamento de Física de Partículas, Univ. of Santiago de Compostela, 15782, Santiago de Compostela, Spain

different points of the collision region. In this sense, anisotropic flow is a particularly unambiguous and strong manifestation of collective dynamics in heavy ion collisions [10]. The large elliptic flow v_2 can be qualitatively understood as follows: In a collision at high energy, the spectators are fast enough to free the way, leaving behind at mid-rapidity an almond shaped azimuthally asymmetric region of QCD matter. This spatial asymmetry implies unequal pressure gradients in the transverse plane, with a larger density gradient in the reaction plane (in-plane) perpendicular to it. As a consequence of the subsequent multiple interactions between degrees of freedom, this spatial asymmetry leads to an anisotropy in momentum space; the final particle transverse momentum are more likely to be in-plane than out-plane, hence $v_2 > 0$ as it was predicted [11].

The experimental results show that the elliptical flow first increases with p_T and then levels off around $p_T \sim 2$ GeV. Also, the p_T -dependent v_2 of identified hadrons shows mass ordering at small p_T and displays a constituent-quark counting rule. On the other hand v_2 normalized to the eccentricity scales on the density of produced charged particles to the overlapping area of the collision. To understand these experimental results, many theoretical approaches have been used. These include hydrodynamics models [12], transport models [13], and hybrid models which combines both hydrodynamic and transport models [14]. Hydrodynamics models usually gives the largest elliptical flow.

In transport models, including the parton cascade [15], it is obtained a sizable v_2 only if it is used a very large parton cross section. On the other hand, transport or hybrid models based on string degrees of freedom in general gives a smaller elliptic flow than the observed at RHIC [16].

The inclusion of interaction among strings via string fusion as in the AMPT model[17], in dual parton model [18] in the quark gluon string model [19] or in Reggeon theory [20] yield a large elliptic flow. In this paper, we would like to study this point further, using percolation of strings. In this model, is introduced the interaction between many degrees of freedom. In fact the overlapping of the strings forming color clusters, can be seen as an interaction among the partons of the projectile and target, from which the strings are stretched. The recombination of the flavour and color of these partons give rise to the flavours and color content of the resulting cluster. Due to that, the fragmentation of the clusters is different of the fragmentation of the initial strings, corresponding to a higher color and also different flavour. This fact, gives rise to a suppression of the multiplicities, a moderate increase

of the transverse momentum and an increase of the ratio baryon/meson with centrality. Also it provide us with an state which has strongly interacted in the first initial times. The percolation of strings incorporates in a dynamical way two of the main features of AA collisions, namely recombination and the formation of a strong interacting partonic system. We will compare the results obtained for the elliptic flow with experimental RHIC data on AA collisions, including the dependence of the nuclear modified factor on the azimuthal angles for different transverse momentum. We will show our predictions for LHC energies, which gives a slightly larger elliptic flow for all particles. A proton can be considered as an extended object, although of smaller size than a nucleus. In proton- proton collisions at LHC energies a high number of strings are stretched between the partons of similar effects to those seen at RHIC experiments could be expected.

At first sight the difference between p_T spectra observed in pp and AA collisions at RHIC energy would suggest little flow, a conclusion in line with naive expectations. However, it has been shown [21] that the effects of energy and momentum conservation actually dominate the observed systematic and that pp collisions may be much more similar to heavy ion collisions than generally thought. In the framework of percolation of strings we derived an approximate analytical formula for the p_T distributions, valid for AA and pp collisions. Using this formula we compute the elliptic flow for pp collisions, at LHC energy, obtaining a sizable size. This is not unexpected because the string density at LHC energy in pp collisions is close to the critical percolation density and therefore there are many strings which overlap each other, giving rise to high density partonic medium.

The plan of the paper is as follows: In the next section, we introduce the percolation of strings, computing the elliptic flow in section 3. In section 4 we discuss our results comparing with the RHIC data and show our predictions at LHC, for AA and pp collisions. Finally we present our conclusions.

2 The string percolation model

In the string percolation model [22] [23] [24], multiparticle production is described in terms of color strings stretched between the partons of the projectile and the target. These strings decay into new ones by $q\bar{q}$ or $qq + \bar{q}\bar{q}$ pair production and subsequently hadronize to produce hadrons. Due to the confinement, the color of these strings is confined to small area in transverse

space $S_1 = \pi r_0^2$ with $r \simeq 0.2 - 0.3$ fm. These values comes from lattice results on bilocal correlators [25] and from the method of field correlators [26] [27] and corresponds to the correlation length of the QCD vacuum. With increasing energy and/or atomic number of the colliding particles, the number of strings, N_s , grows and they start to overlap forming clusters, very much like disks in two dimensional percolation theory. At a certain critical density, a macroscopical cluster appears, which marks the percolation phase transition. This density corresponds to the value $\rho_c = 1.18 - 1.5$, (depending on the type of employed profile functions of the nucleus, homogeneous or Wood-Saxon [28]) where $\rho = N_s S_1 / S_A$ and S_A stands for the overlapping area of the colliding objects. The percolation theory governs the geometrical pattern of the string clustering. Its observable implications, however, require the introduction of some dynamics in order to describe the behavior of the cluster formed by several overlapping strings. We assume that a cluster of n strings behaves as a single string with an energy-momentum that corresponds to the sum of the energy-momenta of the individual strings and with a higher color field, corresponding to the vectorial sum of the color field of each individual string. In this way [29], we can compute the mean multiplicity μ_n and the mean transverse momentum squared $\langle p_T^2 \rangle_n$ of the particles produced by a cluster.

$$\langle \mu_n \rangle = \sqrt{\frac{n S_n}{S_1}} \langle \mu_1 \rangle \quad \text{and} \quad \langle p_{Tn}^2 \rangle = \sqrt{\frac{n S_1}{S_n}} \langle p_{T1}^2 \rangle, \quad (1)$$

where $\langle \mu_1 \rangle$ and $\langle p_{T1}^2 \rangle$ are the mean multiplicity and mean p_T^2 of particles produced by a single string. We take S_1 constant equal to a disc of radius r_0 . S_n corresponds to the total area occupied by n discs, which of course can be different for different configurations even if the clusters have the same number of strings. Notice that if the strings are just touching each other $S_n = n S_1$ and the strings act independently to each other. On the contrary if they fully overlap $S_n = S_1$ it is obtained the largest suppression of the multiplicities and the largest increase of the transverse momentum. In the limit of high density, one obtains [29]

$$\langle n \frac{S_1}{S_n} \rangle = \frac{\rho}{1 - e^{-\rho}} = \frac{1}{F(\rho)^2} \quad (2)$$

and the equations (1) transform into the analytical ones.

$$\langle \mu \rangle = N_s F(\rho) \langle \mu_1 \rangle, \quad \text{and} \quad \langle p_T^2 \rangle = \frac{\langle p_{T1}^2 \rangle}{F(\rho)} \quad (3)$$

with $F(\rho) = \sqrt{\frac{1-e^{-\rho}}{\rho}}$. In principle, the equality (3) has been obtained in the high energy limit, what means close or above, the critical density, where the strings covers a large fraction of the total available area. However the equations (3) give also the right behavior in the limit of low density. In fact if ρ tends to zero, $F(\rho)$ is one and therefore there is not any change from the result of the superposition of individual strings. In the mid rapidity region, the number of strings is proportional to the number of collisions, $N_{coll} \sim N_A^{\frac{4}{3}}$ being N_A the number of participants. Therefore $\rho \sim N_A^{\frac{2}{3}}$ and $\mu \sim N_A$. In other words, the multiplicity per participant becomes independent of N_A , i.e. saturates. Outside the mid rapidity, N_s is proportional to N_A instead of $N_A^{\frac{4}{3}}$. Therefore, there is an additional suppression factor $N_A^{\frac{1}{3}}$ compared to central rapidity.

If we are interested in a specific kind of particle i , we will use equations (1) and (3) μ_{1i} , $\langle p_{T1}^2 \rangle_i$, $\langle \mu_n \rangle_i$ and $\langle p_{Tn}^2 \rangle_i$ for the corresponding quantities.

In order to compute the multiplicities we must know, N_s and μ_1 (for a fixed centrality, knowing N_s we deduce the density ρ). Up to RHIC energies, N_s in the central rapidity region is approximately twice the number of collisions, N_{coll} . However N_s is larger than N_{coll} at RHIC and LHC energies.

Using equation (3) the multiplicities are computed using a Monte-Carlo code based on the Quark- Gluon String model to generate the strings [30]. Each string is produced at an identified impact parameter. From this, knowing the transverse area of each string, we identify all the clusters formed in each collision and subsequently compute for each of them its multiplicity in units of μ_1 the value of μ_1 was fixed by the comparison of our results with SPS data for Pb-Pb central collisions. Our results are in agreement with SPS and RHIC multiplicity data [31]. Using the first of equations(1) we obtain very similar results [32]. Most of the reasonable string models [30] [33][34] [35][36] obtained similar results for N_s . This fact gives us confidence in our values. Notice that sometimes, even in experimental analysis, N_{coll} is obtained from the optical approximation of the Glauber model without taking into account the energy-momentum conservation. This conservation reduces N_{coll} . In the evaluation of the elliptical flow, we need the values of dN/dy at central rapidity for the different collisions and centralities, and values of ρ . We take both from our previous results [31][32].

Concerning the transverse momentum distribution, one needs the distri-

bution $g(x, p_T)$ for each cluster, and the mean squared transverse momentum distribution of the clusters $W(x)$, where x is the inverse of the mean of the transverse momentum of each cluster which is related to the cluster size by equation (3). For $g(x, p_T)$ we assume the Schwinger formula, $g(x, p_T^2) = \exp(-p_T^2 x)$ [23] [37] used also as a first approximation for the fragmentation of Lund string [36]. For the weight function, we assume the gamma distribution $W(x) = \frac{\gamma(\gamma x)^{k-1}}{\gamma(k)} e^{-kx}$, [38] [39] with $\gamma = \frac{k}{\langle x \rangle}$ and $\frac{1}{k} = \frac{(\langle x^2 \rangle - \langle x \rangle^2)}{\langle x \rangle^2}$ is proportional to the width of the distribution, depending on the density of strings η . Therefore the transverse momentum distribution $f(p_T, y)$ of the particle i is

$$\begin{aligned}
 f(p_T, y) &= \frac{dN}{dp_T^2 dy} = \int_0^\infty dx W(x) g(p_T, x) \\
 &= \frac{dN}{dy} \frac{k-1}{k} \frac{1}{\langle p_T^2 \rangle_{>1i}} F(\rho) \frac{1}{(1 + F(\rho) p_T^2 / k \langle p_T^2 \rangle_{>1i})^k} \quad (4)
 \end{aligned}$$

The equation (4) is valid for all types of collisions and high densities. The equations (4) can be seen as superposition of color sources, clusters, where $\frac{1}{k}$ fixes the transverse momentum fluctuations. At small density of strings, there will not be overlapping of strings, the strings are isolated and $k \rightarrow \infty$. When ρ increases, there are some overlapping of strings, forming clusters and therefore k decreases. The minimum of k will be reached when the fluctuations reaches its maximum. Above this point, increasing ρ , these fluctuations decrease and k increases. In the limit of $\rho \rightarrow \infty$, there is only one cluster formed by all the produced strings. Again, there are no fluctuations and k tends to infinity.

The quantitative dependence of k on ρ was obtained in [38] from the comparison of equation (4) with RHIC AA data at different centralities. We use here such a dependence. The peripheral Au-Au collisions at $\sqrt{s} = 200$ GeV, corresponds to the ρ values slightly above the minimum of k [38]. In the range of the used ρ values, k is a smooth function on ρ . We will show that for $p_T < 1.5$ GeV/c our v_2 does not depend on k . The formula (4) is able to describe the transverse momentum distribution for mesons in AA collisions at all centralities and energies up to moderate p_T , $p_T < 4-5$ GeV/c. In particular they describe rightly the Cronin effect and the suppression of moderate p_T particles, as it was shown in reference [38].

We do not claim to describe the data at high p_T . It is well known that jet quenching is the mechanism responsible for the high p_T suppression. This

phenomena is not included in our formula (4) which was obtained assuming a single exponential for the decay of a cluster without a power like tail. Our formula can be seen as a way to join smoothly the low and moderate p_T region with the high p_T region. Indeed, the high p_T suppression implies by continuity a suppression of the highest p_T values of the intermediate region which are described by formula (3).

The universal formula (4) must be considered as an analytical approximation to a process that consists on the fragmentation of clusters of strings and their eventual decay via successive cluster breaking via Schwinger mechanism [40]. The formula (4) is not able to explain the differences between antibaryons (baryons) and mesons. In fact, the only parameter that is different for them in (4) is the mean of the squared of transverse momentum of pions and protons produced by a single string $\langle p_T^2 \rangle_{1\pi}$ and $\langle p_T^2 \rangle_{1p}$, respectively. This only causes a shift on the maximum of R_{AA} but keeps the same height at the maximum contrary to what one observed. However, in the fragmentation of a cluster formed by several strings, the enhancement of production of antibaryons (baryons) over mesons is not only due to a mass effect corresponding to a higher tension due to a higher density of the cluster (the factor $F(\rho)$ in front of p_T^2 in (4)). In fact, the color and flavour properties of a cluster follow from the corresponding properties of their individual strings. A cluster composed by several quark-antiquarks ($q - \bar{q}$) strings behaves like an string with a color Q and flavour composed of the flavour of the individual strings, as a result, we obtain clusters with higher color and different flavour ends. For the fragmentation of a cluster we consider the creation of a pair of parton complex as $Q\bar{Q}$ [40], after the decay, the two new $Q\bar{Q}$ strings are treated in the same manner and therefore decay into more $Q\bar{Q}$ strings, until they come to objects with masses comparable to hadron masses, which are identified with observable hadrons by combining with them the produced flavour with statistical weights. In this way, the production of antibaryons (baryons) is enhanced with the number of strings of the cluster. The additional antiquarks (quarks) required to form an antibaryon (baryon) are provided by the antiquarks (quarks) of the overlapping strings that form the cluster [40][41]. Therefore recombination or coalescence mechanism [42][43] are incorporated in a dynamical way. In order to take this into account keeping our close formula we will do the following approximation. For antibaryons (baryons) we consider instead of the equation (3),

$$\mu_{\bar{B}} = N_s^{1+\alpha} F(\rho_{\bar{B}}) \mu_{1\bar{B}} \quad (5)$$

fitting the parameter α to reproduce the experimental dependence of the p_T integrated \bar{p} spectra with centrality [39]. The obtained value is $\alpha = 0.09$. this means that the density ρ must be replaced by $\rho_B = N_s^\alpha \rho$ The antibaryons (baryons) probe a higher density than mesons for the same energy and type of collision. The equation (4) with the described modification for baryons provide us the input for the evaluation of the elliptic flow.

3 Elliptic Flow.

In saturation initial state models as the color Glass Condensate [44] [45] or the Percolation String Model [22] [23] color sources radially emit particles. The azimuthal asymmetry has, in this case, the origin in the deviation from the circle of the impact parameter projected interacting overlap region in non central, $b > 0$, collisions. The situation is schematically represented in Fig. 1. If one measures production within fixed azimuthal angles, one has to know the source density as a function of R_φ . If no azimuthal determinations are made one can adopt a circle of radius R such that

$$\frac{\pi R^2}{4} = \frac{1}{2} \int_0^{\frac{\pi}{2}} R_\varphi^2 d\varphi \quad (6)$$

or

$$R^2 = \langle R_\varphi^2 \rangle \quad (7)$$

Note that, as in the experiment, we are using for the range of variation of φ , $0 < \varphi < \frac{\pi}{2}$. As the number of color sources is the same in the interior of the circle and in the ellipsoid and as the directional density is related to the average density by the formula

$$\rho_\varphi = \rho \left(\frac{R}{R_\varphi} \right)^2 \quad (8)$$

one expects higher $\langle p_T^2 \rangle$ and larger particle numbers for production in the reaction plane, $\varphi = 0$. In order to make this point clear let us consider a model, simpler than (4), which is the Schwinger model with percolation [37]:

$$\frac{2}{\pi} \frac{dN}{dp_T^2} \sim e^{-F(\rho) \frac{p_T^2}{\langle p_T^2 \rangle > 1}} \quad (9)$$

for the azimuthal integrated cross section and

$$\frac{dN}{dp_T^2 d\varphi} \sim e^{-F(\rho_\varphi) \frac{p_T^2}{\langle p_T^2 \rangle_1}} \quad (10)$$

for a direction φ . From (9) and (10) one sees that the ratio of the p_T integrated quantities is

$$\frac{(10)}{(9)} = \frac{\langle p_T^2 \rangle_\varphi}{\langle p_T^2 \rangle} = \frac{F(\rho)}{F(\rho_\varphi)} \quad (11)$$

which for small φ , as $F(\rho)$ is decreasing function of ρ , is larger than 1. The same result works for Eq. (4). The relevant directional factor is the factor $F(\rho)p_T^2$ or $F(\rho_\varphi)p_T^2$. Let us define, for a given centrality, number of participants or ρ ,

$$\frac{dn}{dy dp_T^2} \Big|_{y=0} \equiv f(F(\rho), p_T^2) \quad (12)$$

and

$$\frac{dn}{dy dp_T^2 d\varphi} \Big|_{y=0} \equiv f(F(\rho_\varphi), p_T^2) \quad (13)$$

We will treat the azimuthal distribution as perturbation around the average, isotropic distribution. Such expansion, as ρ (is proportional) to $\frac{1}{R^2}$ and ρ_φ to $\frac{1}{R_\varphi^2}$, can be written as:

$$f(F(\rho_\varphi), p_T^2) \simeq \frac{2}{\pi} f(F(\rho), p_T^2) \left[1 + \frac{\partial \ln f(p_T^2, R^2)}{\partial R^2} (R_\varphi^2 - R^2) \right] \quad (14)$$

Note that (4), because of (6), satisfies the normalization condition,

$$\int_0^{\pi/2} f(F(\rho_\varphi), p_T^2) d\varphi = f(F(\rho), p_T^2) \quad (15)$$

Additional terms in the expansion will, in general, violate the normalization condition (15). As a decrease in R^2 corresponds to an increase in source density and an increase in particle production one expects, in (16)

$$\frac{df(F(\rho), p_T^2)}{dR^2} < 0 \quad (16)$$

with the consequence, again see (16), that production is maximal for $\varphi \sim 0$. Note that the second term in the right hand side of (16), changes sign at $R_\varphi = R^2$.

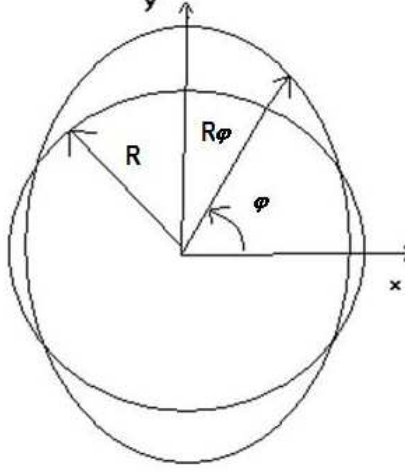


Figure 1:

We shall next write expressions for relevant measurable quantities as modification factors, R_{AA} and v_2 . With the usual definition for $R_{AA}(p_T^2)$, we define,

$$\begin{aligned}
 R_{AA}(p_T^2, \Delta\varphi) &\equiv \Delta\varphi \frac{f_{AA}(F(\rho_\varphi)p_T^2)}{\langle N_{coll} \rangle f_{pp}(F(\rho)p_T^2)} \\
 &= \Delta\varphi R_{AA}(p_T^2) \left[1 + \frac{\partial \ln f_{AA}(F(\rho), p_T^2)}{\partial R^2} (R_\varphi^2 - R^2) \right] \quad (17)
 \end{aligned}$$

and

$$v_2(p_T^2) = \frac{2}{\pi} \int_0^{\frac{\pi}{2}} d\varphi \cos(2\varphi) \left[1 + \frac{\partial \ln f_{AA}(F(\rho), p_T^2)}{\partial R^2} (R_\varphi^2 - R^2) \right] \quad (18)$$

Note that (16), using (4), becomes

$$f(p_T^2, R_\varphi^2) = f(p_T^2, R^2) \left[1 + \frac{1}{R^2 F(\rho)} (e^{-\rho} - F(\rho)^2) \frac{p_T^2}{2p_1^2} \frac{1}{1 + \frac{F(\rho)p_T^2}{kp_1^2}} (R_\varphi^2 - R^2) \right] \quad (19)$$

From the equations (19), (20), (21) we can compute our main observables to compare with the experimental data. The approximation done is valid when

the second term in (21) is small, what means not high p_T . Notice that due to the location in impact parameter space of the strings that form clusters there is an initial spatial azimuthal asymmetry which is translated into transverse momentum due to interactions of strings included in the formula for the p_T distribution via the factor $F(\rho)$. The strength of the interaction depends locally on the string density and therefore is the origin of the azimuthal asymmetry.

4 Results and Discussion

In order to compute the elliptic flow, we need the values of N_s , ρ , $k(\rho)$ and $\langle p_T^2 \rangle_{1\pi}$, $\langle p_T^2 \rangle_{1k}$, $\langle p_T^2 \rangle_{1\bar{p}}$. As we mentioned before, for each type of collision, energy and centrality, we obtain the number of strings using a Monte-Carlo code based on the Quark Gluon string model [30], hence we compute ρ and $k(\rho)$. The dependence of k on ρ is very smooth, our results for $p_T < 1.0$ GeV/c are independent of k according to formula (18) and (19). In table 1, we show the value of N_s , ρ , $k(\rho)$ for different types of collisions, centralities and energies. We include also the values of the charged multiplicity at central rapidity $\frac{dN}{dy}$ which we will use below. They are taken from previous work done in the framework of percolation [31] [32] [37][46]. We use the values $\langle p_T^2 \rangle_{1\pi} = 0.06(\text{GeV}/c)^2$, $\langle p_T^2 \rangle_{1k} = 0.14(\text{GeV}/c)^2$, $\langle p_T^2 \rangle_{1\bar{p}} = 0.30(\text{GeV}/c)^2$, obtained previously from the comparison of formula (4) with the experimental data of the dependence of the mean transverse momentum of the different particles on the multiplicity [37] [38].

Once these parameters are fixed then the elliptic flow for a certain type of collision, centrality and energy is known because it only depends on ρ . Notice, that we could consider $\langle p_T^2 \rangle_{1\pi}$, $\langle p_T^2 \rangle_{1k}$, $\langle p_T^2 \rangle_{1\bar{p}}$ as free parameters doing a fit to the experimental data. However, our aim is not to obtain a perfect agreement with data. We are aware of some simplifications and limitation of our framework, therefore we just check whether the general trend of the data is reproduced in our model.

In fig. 2 we show our results for minimum bias Au-Au collisions for pions, kaons and antiprotons compared with the experimental data [47]. A reasonable agreement is obtained for $p_T \leq 1$ GeV/c, reproducing the mass ordering. In fact, at low p_T , the elliptic flow is proportional to p_T^2 and the proportionality coefficient is $\frac{1}{\langle p_{T1}^2 \rangle_{\pi}}$. As $\langle p_{T1}^2 \rangle_{\pi} < \langle p_{T1}^2 \rangle_k < \langle p_{T1}^2 \rangle_{\bar{p}}$ v_2 is larger for pions than for kaons and antiprotons. Our evaluation was

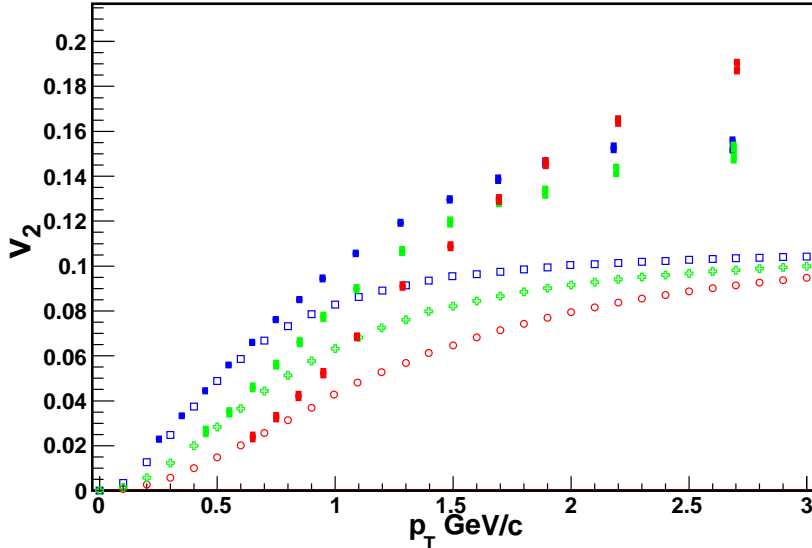


Figure 2: Elliptic flow for different hadron species in Au+Au collisions, color lines in red, blue and green show our predictions, for antiprotons, pions and kaons respectively, dashed lines experimental data from RHIC [48].

done retaining only the first term of the expansion in powers of $R_\phi - R$. For $p_T < 1.5$ GeV/c, this term is small, however for larger p_T we should include additional terms.

In fig. 3 we compare our results on the azimuthal angle dependence of the nuclear modified factor $R_{AA}(p_T^2, \Delta\varphi)$ at different centralities with the PHENIX experimental data [49]. The model reproduces the shape for all centralities although the results are below the experimental data for low angles.

In fig. 4 we plot v_2/ϵ_{part} being $\epsilon = \frac{\sqrt{(\sigma_y^2 - \sigma_x^2)^2 + 4(\sigma_{xy})^2}}{\sigma_x^2 + \sigma_y^2}$ the participant eccentricity as a function of the number of participants N_A together the PHOBOS [50][51] experimental data in Cu-Cu and Au-Au at $\sqrt{s} = 200$ GeV. It is observed good agreement.

In fig. 5 we plot v_2/ϵ , being the participant eccentricity as a function of the ratio $\frac{dN_{ch}}{dy} \frac{1}{S}$ where S is the surface of the collision for a given centrality. Together our results we show the experimental data at AGS, SPS and RHIC

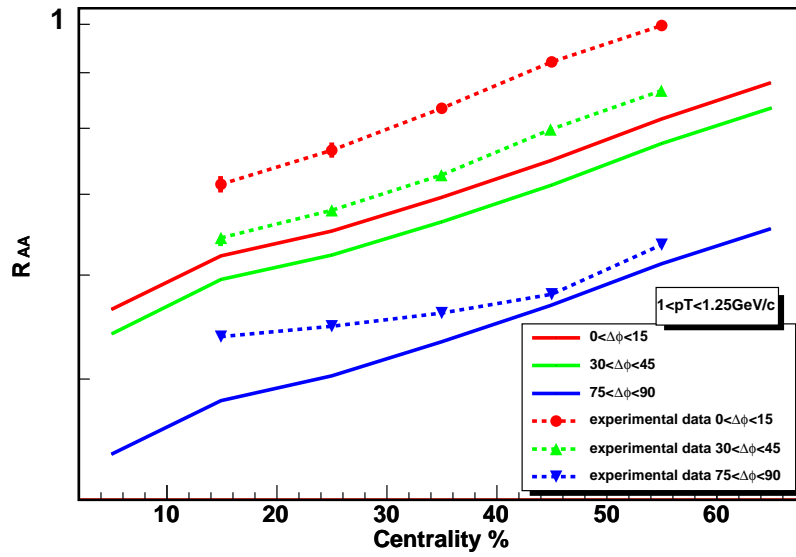


Figure 3: Angular suppression for pions at different centrality, (10–20%, 20–30%, 30–40%, 50–60%) results compared to PHENIX data.

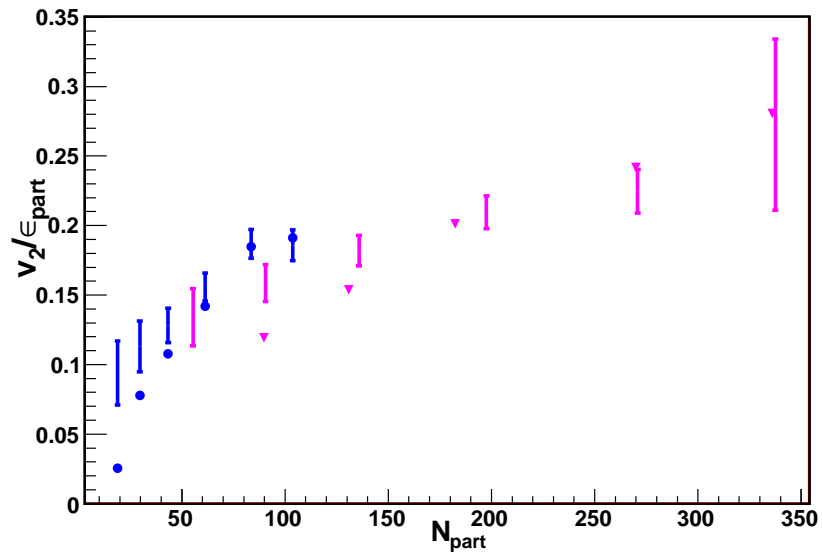


Figure 4: Elliptic flow v_2/ϵ_{part} as a function of the number of participants. Pink triangles and round points are the model results for Au-Au and Cu- Cu collisions at $\sqrt{s} = 200$ GeV.

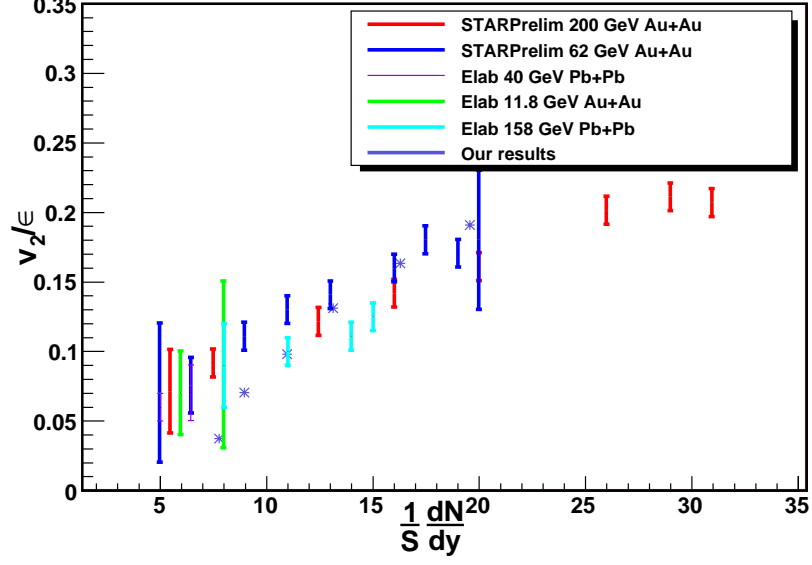


Figure 5: Scaling predictions for Au+Au at $\sqrt{s} = 200$ GeV (stars).

energies for different type of collisions [52]. A good agreement is observed. The scaling, experimentally observed, is also expected in our model. In fact, from equation (2) we obtain.

$$\frac{1}{S} \frac{dN_{ch}}{dy} = \rho F(\rho) \frac{\mu_1}{r_0^2} \quad (20)$$

which is proportional to $\sqrt{\rho}$ at high densities. On the other hand, from equations (22) and (20) we have

$$v_2(p_T) = A \left(\frac{2}{\pi} \int_0^{\pi/2} d\phi \cos(2\phi) \left(\frac{R_\phi^2}{R^2} - 1 \right) \right) \quad (21)$$

with

$$A = \frac{e^{-\rho} - F(-\rho)^2}{F(\rho)} \frac{p_T^2}{2\bar{p}_{T1}^2} \frac{1}{1 + \frac{F(\rho)p_T^2}{2\bar{p}_{T1}^2}} \quad (22)$$

As the bracket of the equation(24) is related to the centrality and A depends only on ρ , i.e. depends only on $\frac{1}{S} \frac{dN_{ch}}{dy}$. The equation (21) gives approximately the scaling law observed.

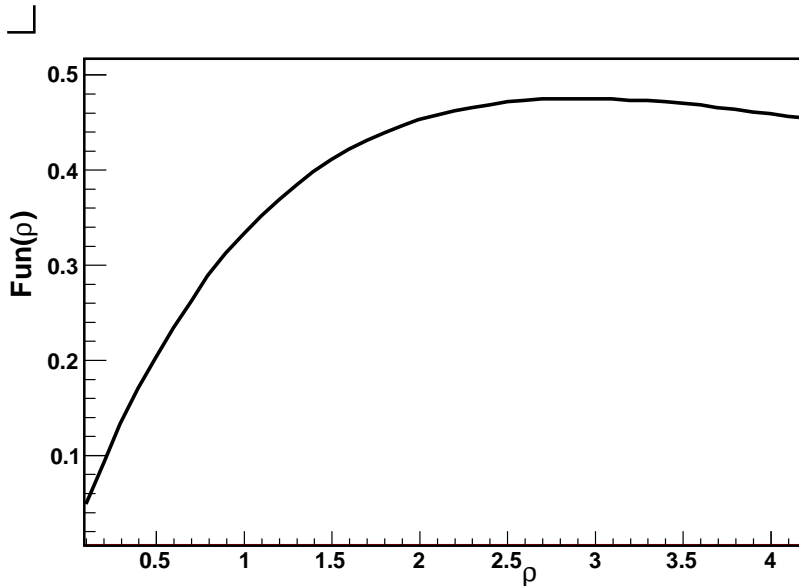


Figure 6: Dependence on the string density of the function described in the text

In fig. 6 we plot the function $-(e^{-\rho} - F(\rho)^2)/F(\rho)$ as a function of ρ . We observe that it increases up to $\rho \approx 2.7$ where it starts to decrease slowly. Therefore we predict this behavior for the elliptic flow. As the value $\rho = 2.5$ only is reached for central Au-Au collisions at RHIC or semicentral at LHC energies, only for this type of collisions will be slightly smaller at LHC energies. As the antibaryons(baryons) probe a higher string density than the mesons the elliptic flow for them will decrease for a less degree of centrality.

In fig. 7 we plot v_2/nq as a function of the kinetic energy over the constituent quarks of the observed particles. The recombination models [42][43] predicted an scaling law for intermediate transverse momentum, independently of mesons or baryons, all particles should lay in the same universal curve. We show our results for pions, kaons and antiprotons together with the experimental data [48]. It is seen that our model satisfies the scaling law as it was expected. In fact, in the percolation of strings, in addition to the mass effect due to a higher tension of the cluster which gives rise to enhancement of heavier particles, there is a flavouring effect related to the number of strings of the cluster, each one with flavour, which gives rise to

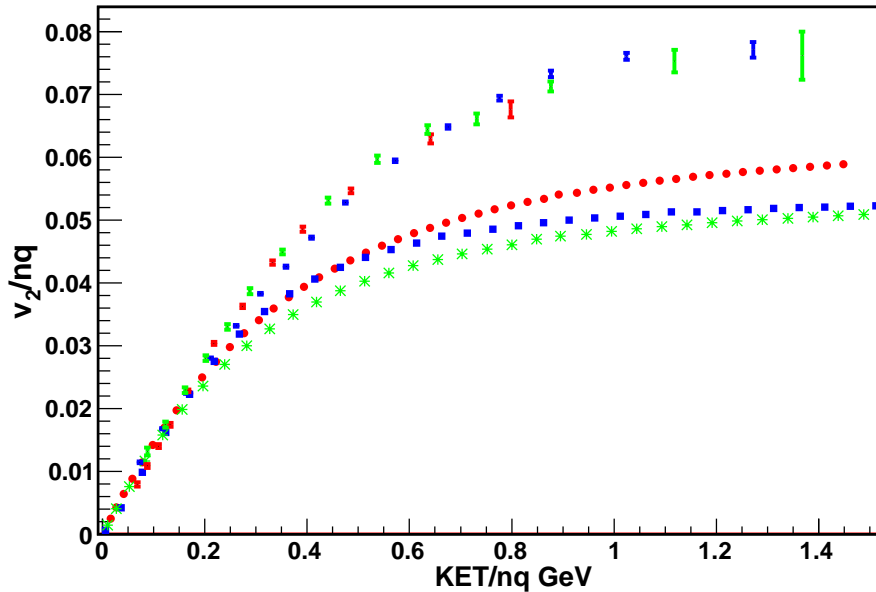


Figure 7: The red, green and blue solid lines stand for the model results for antiprotons, kaons and pions respectively compared with the experimental data (errors are smaller than symbols used).

a higher probability to combine them, producing more baryons [39] [40]. In order to obtain close formula we incorporate this, only in approximate way as was explained before, however our results for pions, kaons and antiprotons are laying approximately in the same curve as the experimental data, for $\text{KeT}/nq < 0.2$ GeV, corresponding to low p_T . For higher p_T the result is below the experimental data.

In figs. 8, 9, 10 we show our results at $\sqrt{s} = 5.5$ TeV compared with $\sqrt{s} = 200$ GeV for different hadrons. For the three particles we obtain a moderate increase of elliptic flow. This is a consequence that the string density at both energies for minimum bias Au-Au collisions is below 2.7. Above this density, the elliptic flow decreases what happened for Pb-Pb central collisions at LHC.

In fig. 11 we show our prediction for v_2 for pp collisions at $\sqrt{s} = 14$ TeV for pions and kaons. A sizable elliptic flow is obtained, this result is not

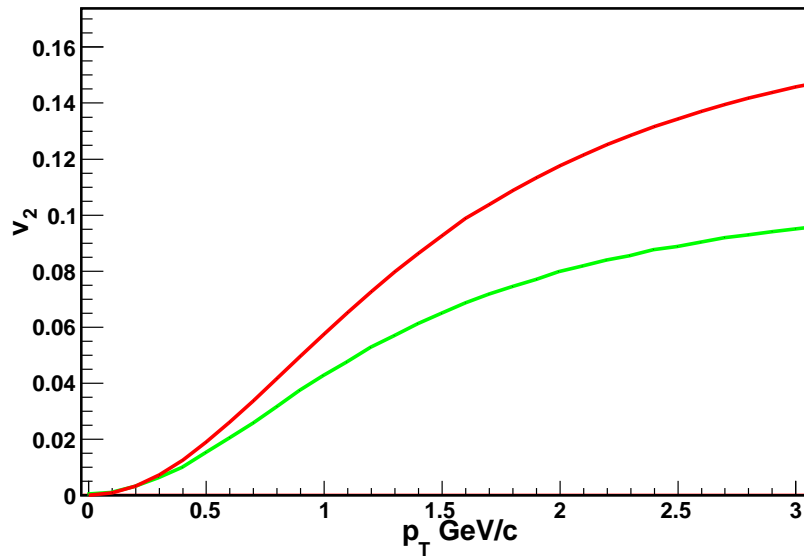


Figure 8: Expected elliptic flow for antiprotons by our model, green lines RHIC and red lines LHC energies.

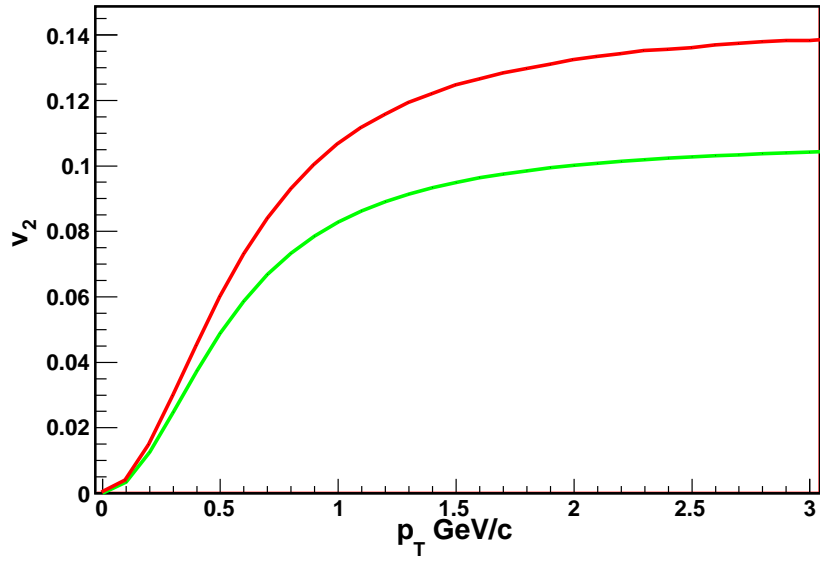


Figure 9: Expected elliptic flow pions by our model, green lines RHIC and red lines LHC energies.

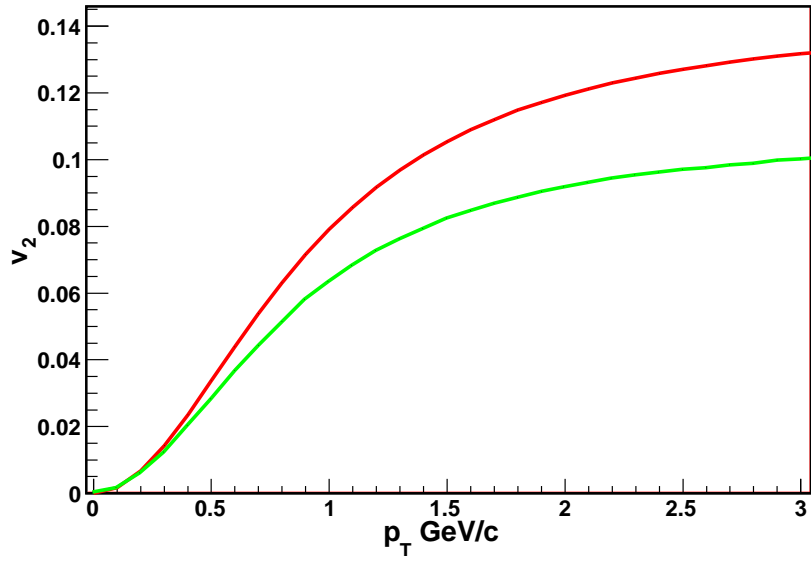


Figure 10: Expected elliptic flow kaons by our model, green lines RHIC and red lines LHC energies.

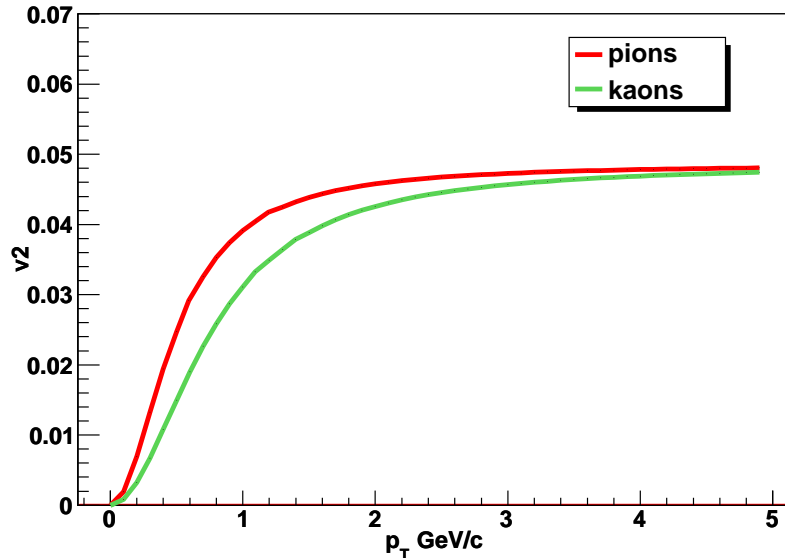


Figure 11: pp predictions at $\sqrt{s} = 14$ TeV.

surprising, given the high density partonic structure obtained in pp at LHC which is similar, see table 1, to Cu-Cu collisions. The high density partonic structure of pp at LHC can give rise to other effects observed in AA collisions at RHIC as the high p_T particles and the existence of large rapidity long range correlation even at very large intervals of rapidity [53][54][55].

5 Conclusions.

In the framework of the clustering of color sources, the elliptic flow, v_2 , and the dependence of the nuclear modified factor on the azimuthal angle have been evaluated.

The comparison with RHIC experimental data for $p_T < 1.5$ GeV/c shows a reasonable agreement. In particular, the observed mass ordering is reproduced. In the model, is obtained an analytical expression for the observed scaling of the elliptic flow normalized to the participant eccentricity on the ratio $\frac{1}{S} \frac{dN}{dy}$. The analytical expression indicates that above a determined density $\rho = 2.7$ elliptical flow decreases slowly. This density is reached in Au-Au cen-

tral collisions both at RHIC and LHC energies, therefore we predict slightly decrease in this case. For Au-Au minimum bias the density is lower than 2.7 and we predict a slightly increase in that case.

We have computed the dependence of the nuclear modify factor on the azimuthal angle comparing our results with experimental data for different centralities. We reproduce the general trend of the data, although we are 15% below for small angles.

We predict sizable elliptic flow in proton proton collisions, consequence of the high partonic density reached at LHC energy. The main ingredient of the model is the interaction among strings or equivalently among the partons of projectile and target located at the end of each string. In this way, we have a high density partonic interacting medium. The reasonable agreement obtained in our model with the experimental data for $p_T < 1.5$ GeV/c, confirms the common belief that elliptic flow reveals a strongly interacting medium created in the first stage of the collision. Our predictions will be tested with the incoming LHC experiments.

	N_s	ρ	$k(\rho)$	$\frac{dN}{dy}$
pp (m.b)	8	0.4	3.6	2.5
-	14	0.7	3.4	5.5
Cu-Cu (m.b)	100	0.4	3.6	50
-	170	0.7	3.4	120
Au-Au (m.b)	390	1.0	3.6	180
-	550	1.6	3.6	400
Au- Au (0 – 10)%	1600	2.7	4.0	650
-	2600	4.8	4.1	1500

Table 1: Values of N_s , ρ , $k(\rho)$ and $\frac{dN}{dy}$ for pp, Cu-Cu, Au-Au minimum bias (m.b) and 0 – 10% central Au-Au collisions. For each collision the above numbers correspond to $\sqrt{s} = 200$ GeV and the below ones to $\sqrt{s} = 5.5$ TeV.

Acknowledgements

We thank Dr. N. Armesto and Dr. Carla Vale for discussions.

J. D. D. thanks the support of the FCT/Portugal project PPCDT/FIS/575682004.

I. B, L. C. and C. P. were supported by the project FPA2008-01177 of MICINN, the Spanish Consolider Ingenio 2010 program CPAN and Conselleria Educacion Xunta de Galicia.

References

- [1] K. Adcox *et al.* [PHENIX Collaboration], Nucl. Phys. A **757** (2005) 184.
- [2] J. Adams *et al.* [STAR Collaboration], Nucl. Phys. A **757**, 102 (2005).
C. Adler *et al.* [STAR Collaboration], Phys. Rev. Lett. **87**, 182301 (2001).
- [3] S. Manly *et al.* [PHOBOS Collaboration], Nucl. Phys. A **774**, 523 (2006).
- [4] K. Adcox *et al.* [PHENIX Collaboration], Phys. Rev. Lett. **89**, 212301 (2002)
- [5] S. S. Adler *et al.* [PHENIX Collaboration], Phys. Rev. Lett. **94**, 232302 (2005)
- [6] C. Adler *et al.* [STAR Collaboration], Phys. Rev. Lett. **87**, 182301 (2001)
- [7] J. Adams *et al.* [STAR Collaboration], Phys. Rev. Lett. **92**, 052302 (2004) Phys. Rev. Lett. **93**, 252301 (2004)
- [8] B. B. Back *et al.* [PHOBOS Collaboration], Phys. Rev. C **72**, 051901 (2005)
- [9] B. Alver *et al.* [PHOBOS Collaboration], Phys. Rev. Lett **98**, 242302 (2007)
- [10] N. Borghini and U. A. Wiedemann, J. Phys. G **35**, 023001 (2008).
- [11] J. Y. Ollitrault, Phys. Rev. D **46**, 229 (1992).
- [12] P. Huovinen, P. F. Kolb, U. W. Heinz, P. V. Ruuskanen and S. A. Voloshin, Phys. Lett. B **503**, 58 (2001).
- [13] L. Bravina, K. Tywoniuk, E. Zabrodin, G. Burau, J. Bleibel, C. Fuchs and A. Faessler, Phys. Lett. B **631**, 109 (2005).
- [14] D. Teaney, J. Lauret and E. V. Shuryak, Phys. Rev. Lett. **86**, 4783 (2001). T. Hirano, U. W. Heinz, D. Kharzeev, R. Lacey and Y. Nara, Phys. Rev. C **77**, 044909 (2008).
- [15] D. Molnar and M. Gyulassy, Nucl. Phys. A **698**, 379 (2002).

- [16] M. Bleicher and X. Zhu, Eur. Phys. J. C **49**, 303 (2007).
- [17] Lin Z W and Ko C M Phys. Rev. C 65 034904, (2002); Chen L W and Ko C M Phys. Lett. B 634 205,(2006)
- [18] F. W. Bopp, J. Ranft, R. Engel and S. Roesler, [arXiv:hep-ph/0403084].
- [19] J. Bleibel, G. Baur, A. Faessler and C. Fuchs, Phys. Rev. C **76**, 024912 (2007).
- [20] K. G. Boreskov, A. B. Kaidalov and O. V. Kancheli, Phys. Atom. Nucl. **72** (2009) 361 [Yad. Fiz. **72** (2009) 390].
- [21] Z. Chajecski and M. Lisa, Phys. Rev. C **79**, 034908 (2009)
- [22] N. Armesto, M. A. Braun, E. G. Ferreira and C. Pajares, Phys. Rev. Lett. **77**, 3736 (1996). M. Nardi and H. Satz, Phys. Lett. B **442**, 14 (1998).
- [23] C. Pajares, Eur. Phys. J. C **43**, 9 (2005). J. Dias de Deus and R. Ugoccioni, Eur. Phys. J. C **43**, 249 (2005).
- [24] H. J. Moring, J. Ranft, C. Merino and C. Pajares, Phys. Rev. D **47**, 4142 (1993).
- [25] M. Campostrini, A. Di Giacomo and G. Mussardo, Z. Phys. C **25**, 173 (1984). M. Campostrini, A. Di Giacomo and S. Olejnik, Z. Phys. C **31**, 577 (1986).
- [26] H. G. Dosch and Yu. A. Simonov, Phys. Lett. B **205**, 339 (1988).
- [27] A. Di Giacomo, H. G. Dosch, V. I. Shevchenko and Yu. A. Simonov, Phys. Rept. **372**, 319 (2002)
- [28] A. Rodrigues, R. Ugoccioni and J. Dias de Deus, Phys. Lett. B **458**, 402 (1999)
- [29] M. A. Braun and C. Pajares, Phys. Rev. Lett. **85**, 4864 (2000)
M. A. Braun and C. Pajares, Eur. Phys. J. C **16**, 349 (2000)
- [30] N. S. Amelin, N. Armesto, C. Pajares and D. Sousa, Eur. Phys. J. C **22**, 149 (2001)

- [31] M. A. Braun, F. Del Moral and C. Pajares, Phys. Rev. C **65**, 024907 (2002)
- [32] J. Dias de Deus and R. Ugoccioni, Phys. Lett. B **494**, 53 (2000) J. D. De Deus and A. Rodrigues, Phys. Rev. C **67**, 064903 (2003)
- [33] A. Capella, U. Sukhatme, C. I. Tan and J. Tran Thanh Van, Phys. Rept. **236**, 225 (1994).
- [34] A. Capella, C. Pajares and A. V. Ramallo, Nucl. Phys. B **241**, 75 (1984).
- [35] K. Werner, Phys. Rept. **232**, 87 (1993).
- [36] B. Andersson, Camb. Monogr. Part. Phys. Nucl. Phys. Cosmol. **7**, 1 Cambridge University Press (1997).
- [37] J. Dias de Deus, E. G. Ferreira, C. Pajares and R. Ugoccioni, Eur. Phys. J. C **40**, 229 (2005).
- [38] J. Dias de Deus, E. G. Ferreira, C. Pajares and R. Ugoccioni, Phys. Lett. B **581**, 156 (2004).
- [39] L. Cunqueiro, J. Dias de Deus, E. G. Ferreira and C. Pajares, Eur. Phys. J. C **53**, 585 (2008)
- [40] N. S. Amelin, M. A. Braun and C. Pajares, Z. Phys. C **63**, 507 (1994).
- [41] N. S. Amelin, M. A. Braun and C. Pajares, Phys. Lett. B **306**, 312 (1993).
- [42] R. C. Hwa and C. B. Yang, Phys. Rev. C **67**, 034902 (2003).
- [43] R. J. Fries, B. Muller, C. Nonaka and S. A. Bass, Phys. Rev. Lett. **90**, 202303 (2003). V. Greco, C. M. Ko and P. Levai, Phys. Rev. Lett. **90**, 202302 (2003).
- [44] L. D. McLerran and R. Venugopalan, Phys. Rev. D **49**, 2233 (1994). L. D. McLerran and R. Venugopalan, Phys. Rev. D **49**, 3352 (1994).
- [45] Y. V. Kovchegov and K. L. Tuchin, Nucl. Phys. A **708**, 413 (2002). Yu. V. Kovchegov, Nucl. Phys. A **715**, 891 (2003).

- [46] P. Brogueira, J. Dias de Deus and C. Pajares, Phys. Rev. C **75**, 054908 (2007)
- [47] S. S. Adler *et al.* [PHENIX Collaboration], Phys. Rev. Lett. **91**, 182301 (2003)
- [48] A. Adare *et al.* [PHENIX Collaboration], Phys. Rev. Lett. **98**, 162301 (2007)
- [49] S. Afanasiev *et al.* [PHENIX Collaboration], arXiv:0903.4886 [nucl-ex].
- [50] B. Alver *et al.* [PHOBOS Collaboration], Phys. Rev. Lett. **98**, 242302 (2007)
- [51] S. S. Adler *et al.* [PHENIX Collaboration], Phys. Rev. C **77**, 014906 (2008)
- [52] S. A. Voloshin [STAR Collaboration], J. Phys. G **34**, S883 (2007)
- [53] L. Cunqueiro, J. Dias de Deus and C. Pajares, arXiv:0806.0523 [hep-ph].
- [54] P. Brogueira, J. Dias de Deus and C. Pajares, Phys. Rev. Lett. **B**, 675, 308 (2009) P. Brogueira, J. Dias de Deus and J. G. Milhano, Phys. Rev. C **76**, 064901 (2007)
- [55] N. Armesto, L. McLerran and C. Pajares, Nucl. Phys. A **781**, 201 (2007)
N. Armesto, M. A. Braun and C. Pajares, Phys. Rev. C **75**, 054902 (2007)